Numerical Prediction of Oil Mineral Aggregates Dispersion in the Estuary Of ST-Lawrence River

Journal of Physics: Conference Series **1743** (2021) 012033 doi:10.1088/1742-6596/1743/1/012033

NUMERICAL PREDICTION OF OIL MINERAL AGGREGATES DISPERSION IN THE ESTUARY OF ST-LAWRENCE RIVER

Bajil Ouartassi [1,3], **Bernard Doyon** [2], [3] **Mourad Heniche**

[1] LIPIM, Sultan Moulay Sliman University, National School of Applied Sciences, Khouribga, Morroco

[2]Canadian Coast Guard - Quebec Region, Department of Fisheries and Oceans Canada,101 Champlain Blvd, Quebec City, QC, Canada G1K 7Y7

[3]URPEI, Department of Chemical Engineering, École Polytechnique de Montréal, PO Box 6079, Stn Centre-Ville, Montreal, QC, Canada H3C3A7

E-mail: b.ouartassi@usms.ma

E-mail: Bernard.Doyon@dfo-mpo.gc.ca

E-mail: mourad.heniche@polymtl.ca

Abstract. As part of the environment of the St-Lawrence River, the Canadian Coast Guard team and the URPEI research team at Ecole Polytechnique de Montreal carried out a numerical simulation based on the Eulerian-Lagrangian formulation for the dispersion of oil-mineral aggregates (OMA) in a turbulent flow produced by a propeller ship. This study is part of a larger project to assess the effectiveness of using fine clay minerals as a natural dispersant of petroleum in ice. The interest is to study the effect of an ice cover on the dispersal potential of a typical winter flow field. To highlight the potential dispersion, two hydrodynamic scenarios are chosen, with and without the presence of an ice cover. For each scenario, the calculation results are presented for a selection of particle densities in order to assess the model by comparison of the OMA distribution statistics in the water column.

1. INTRODUCTION

Clay From an environmental perspective, the struggle to oil spills in rivers. A major concern of the Canadian Coast Guard (CCG) a branch of the Canadian Department of Fisheries and Oceans. Several techniques are used to limit the impact of an oil spill into the environment from which we can consider the use of chemical dispersants or the use of mechanical suction. The presence of ice is however a limiting factor in performance of these techniques.

The possibility of accidental oil spills in the St. Lawrence River during winter remains a significant concern for the CCG. Spill sources come from stevedoring in oil terminals, grounding on sand banks, collisions between ships or with obstacles to name a few. Although their frequency decreased, there are more or less 35 fluvial oil spills per year. The decontamination budget follows at a rate of several thousand dollars per ton. In winter conditions, the impact of an oil spill is all the more important that there exist no effective method of recovering spilled oil when water is encumbered with ice. The traditional mechanical oil recovery methods, deployed because there are no other alternatives, offer a poor performance in ice. As a result, at-sea recovery is very

expensive and ineffective under these conditions.
Part of a venture in scientific co-operation that aims at assessing the effectiveness of using fine clay minerals as natural dispersant of oil in ice, the results of this study will allow the CCG to develop guidelines for an oil spill response procedure in ice-encumbered waters. The response procedure aims at neutralizing oil products by adding fine sediments and to disperse them in the form of oil-mineral aggregates (OMA) which have the property of being easily metabolizable by micro-organisms.
This promising alternative spill countermeasure takes advantage of the natural phenomenon of aggregation of oil droplets to mineral fines, which has proven to play a significant role in the "self-cleaning" of soiled low hydrodynamics energy environment. Also, given the hydrodynamic conditions and chemical characteristics of the water in the St. Lawrence Estuary, researchers came to the conclusion that a response method based on the formation of OMA could prove to be effective when sediments are artificially introduced along with some mixing energy, even when ice is present. That energy will have to be introduced artificially. It was then considered to use the turbulence produced by an ice-breaker?s impellers to generate sufficient mixing to initiate the formation of OMA. However, its dispersion potential is not well understood.
Hence, this study aims at assessing the effectiveness of using fine clay minerals as natural dispersant of oil in ice. The interest is to investigate the influence of an ice cover on the dispersion potential in winter conditions. The OMA drift and fate model is based on a one-way coupling solid-liquid model. A RANS model is used to obtain the turbulent velocity field that was combined to the sedimentation velocity field to build up the hydrodynamic database employed for OMA tracking. To evidence the potential dispersion, two hydrodynamic scenarios are retained, with and without an ice cover on the free surface. For each scenario, the computational results are presented for a selection of particle densities in order to appraise the model through comparison of the statistics of OMA distribution in the water column.
In the light of the results obtained, the following conclusions can be drawn:

- the ice cover influences the OMA distribution pattern.
- the proportion of OMA in the bulk of the water column is larger in winter condition versus ice-free conditions.
- impeller ship rotational speed influences the OMA potential dispersion.

In order to overcome the shortcomings of "traditional" methods of intervention, CCG working to develop an alternative method that takes advantage of the process formation of OMA.
The method aims to break the oil slick into small droplets that the addition of fine sediment is stabilized by forming OMA to be dispersed due to currents generated by the rotating propeller of an icebreaker.
This warrant is ultimately to perform tests of numerical dispersion of OMA in an environment turbulent three-dimensional and subject to various conditions common.
The main objective section is to help identify the conditions under which the method of intervention could be successfully applied, ie with a maximum dispersion of OMA.
First, place the target area as part of this study is the region of Matane presented in Figure 1. This zone covers the St. Lawrence River in an area of 120km long by 80km wide with a depth ranging from 0 to just over 500m.

2. METHODOLOGY

2.1. Selected scenarios hydro sedimentary

The dispersal potential is conditioned not only by the hydrodynamics but also by the sedimentary characteristics of OMA. CCG has provided the hydrodynamic transient field of study. It is strongly influenced by the tide phenomenon and by the nature of the terrain. The seaplane base

Figure 1. St Lawrence in the region of Matane (Quebec - source Google Map).

is used to predict the dispersion of OMA in the wild. We will return in more detail later in this document. In this study, the OMA is characterized by two properties of sedimentary:

- The diameter D_p
- The density d relative to water

In order to perform a simulation of dispersal realistically as possible, 12 classes OMA were selected on the basis of D_p and d. The values of D_p between 50 and 250μm , that of d between 1.01 and 1.15. Table 1 shows the statistical series related to different classes of OMA. It follows a normal distribution assumption for average values $\bar{D}_P = 200\mu m$ and $\bar{d} = 1.07$.

Dp(μm) ($\bar{D}_P = 200\mu m$)	*Density of OMA* ($d = 1.07$)			
50	0.036	0.0555	0.0519	0.0246
125	0.0823	0.27	0.119	0.0563
250	0.0959	0.148	0.138	0.0653

Table 1. Table 1: Probabilities pi under the normal classes OMA deductions

3. METHODOLOGY OF SIMULATION OF THE DISPERSION OMA

3.1. Representation of OMA

In this work we assume that the OMA formed the dispersed phase. Furthermore, we assume that their concentration is sufficiently dilute so that on one hand it does not influence the flow field (low fluid-particle) and other particle-particle collisions are negligible. Because of their small diameter of the order of several microns, the relaxation time of the OMA is small (10-4 s) to consider allowing the inertia and drag negligible.

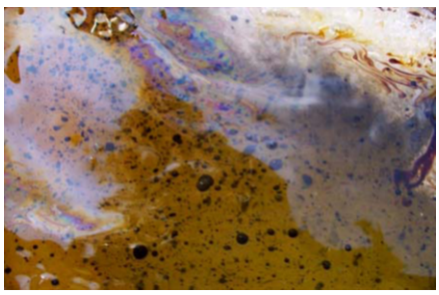

Figure 2. Overview of OMA training).

However, in this work we assume that the particles obey the force of gravity so that the sedimentation can be numerically predicted. Assuming that the time scale of the phenomenon

of sedimentation (several days) is greater than the time scale of turbulence, then we can neglect the contribution of the component of turbulent fluctuation of velocity. Once these assumptions taken into consideration, it expresses the kinematics of OMA as follows:

$$x(t) = x(0) + \int_0^t (u(l) + v_s)dl \tag{1}$$

where $x(0)$ and $x(t)$ are respectively the positions of the OMA at the initial time $t = 0$ and at time t. $u(t)$ is the vector velocity of the river, it depends on time because of the tide. vs $(0.0, vs)$ is the velocity sedimentation working only in the vertical direction z. It's shooting algorithm predictor-corrector $HenicheandTanguy, 2006$ that is retained in this work to solve the equation (1) for the position of the OMA at all times knowing the position of the injection point and the hydrodynamic field. The principle of operation of the algorithm is illustrated in Figure 3. Indeed, consider an OMA occupies the initial time the position Xp in the domain ?e. The principle of the shooting method is to determine the exit point X_Q by a succession of prediction-correction X_Q^i.

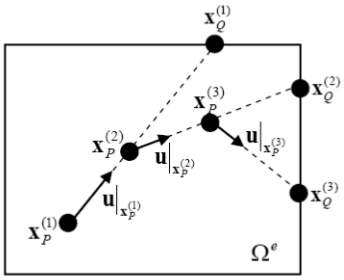

Figure 3. Shooting algorithm predictor-corrector calculation points of the path of an OMA.

This method has the advantage of having no restriction on the time step in contrast to traditional methods of time integration methods such as Runge-Kutta of order 2 and 4 are most used (Cheng et al. 1996). It is worth mentioning that the accuracy of this scheme depends on the number of shots per mesh element hydrodynamics. We return to this aspect in the presentation of results.

4. Seaplane base type tide transient

The river current: the velocity field u(t) according to equation (1), consists of speed values recorded for hours over a period of 24 hours. This velocity field is supported by a set of points 21 in number 600. These are distributed on a regular basis at 300 dots per horizontal layer (XY plane) on a total of 72. Note that the X-axis corresponds to the east and the Y axis to the north. The coast of the z surface layer is at an elevation of-2.5m and the final is-510m. The resolution of equation (1) has been developed to run on a finite element mesh into tetrahedral. We therefore developed a procedure for projecting the velocity field from seed points to a finite element mesh, built on the I-DEAS software (Siemens), composed of 146 725 tetrahedral and 174 301 nodes for a degree of super-linear spatial interpolation type MINI (Arnold et al., 1984). Figure 4 and Figure 5 allow you to view, from an image taken on the software Ensight (CEI), the velocity field respectively at times t and t = 12 hours = 17 hours different coasts z:-2.5m (free surface), and-27.5m-112.5m. On the left column (a) we have the speed on the seeding point while on the right column (b) we have hose on the FE mesh. There is excellent correspondence between the two data sources. We also noted a high variability of the velocity field and a complete reversal of current between the high tide at t=12 hours and the low at t = 17 hours. Areas correspond

to zero speed at exposed areas covered by the grid hydrodynamics. It is therefore entitled to expect a strong influence of hydrodynamic conditions on the dispersion of OMA.

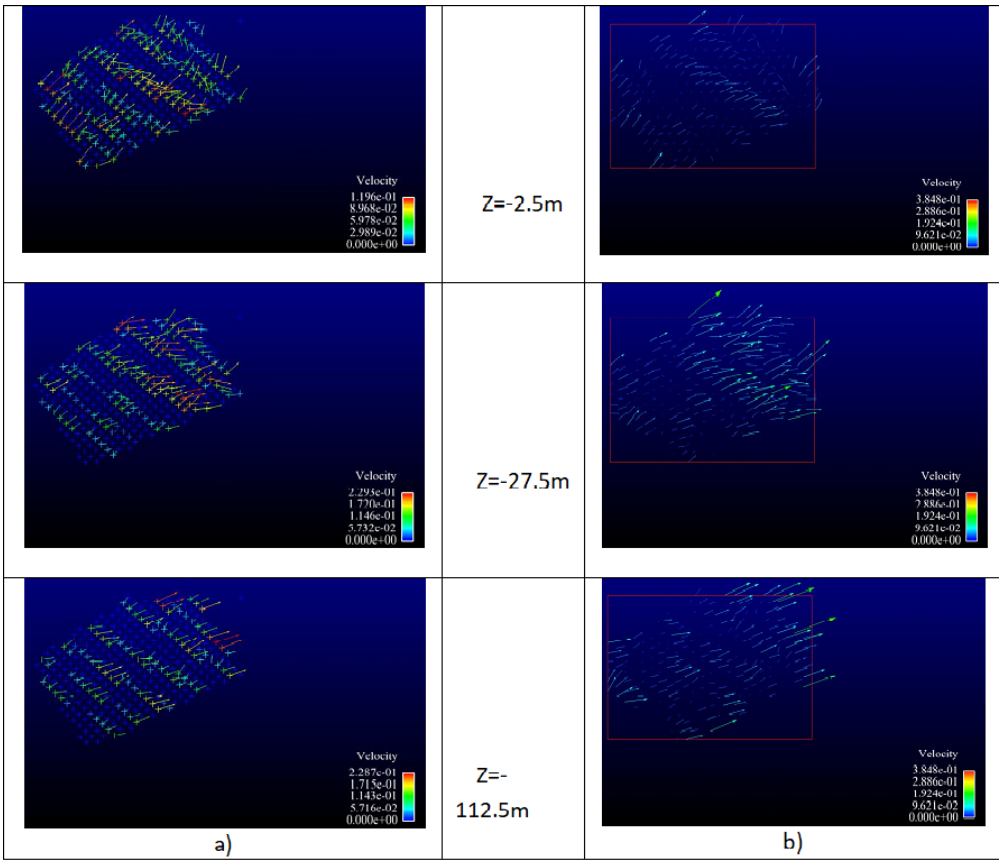

Figure 4. Tidal current at different coasts z at t = 12 hours. a) seeding points b) tetrahedral mesh.

To reduce excessive consumption of computational time by repeated access to the hard disk of the computer to read and interpolate in space-time velocity field, the hydrodynamic field is approximated by a fast Fourier transform (FFT) that can be stored in main memory for better numerical efficiency. In addition, the FFT is well suited for periodic physical phenomena such as tides. TFF field is expressed as follows (Cooley and Tukey, 1965):

$$u_h^i(t) = u_0^i(t) + \sum_{k=1}^{n-1}(a_k^i cos(kt) + b_k^i sin(kt)). \tag{2}$$

Where $u_h^i(t)$ is the effective rate on the hydrodynamic mesh node i at time t. The coefficients a_k^i and b_k^i are the corresponding components of the FFT series and the parameter n is an integer representing the number of harmonics. For periodic flows, the number of harmonics n can be obtained by the relation $n = N/2$, N being the number of time steps to cover a tidal period. In this study $N = 25$ and $n = 13$.

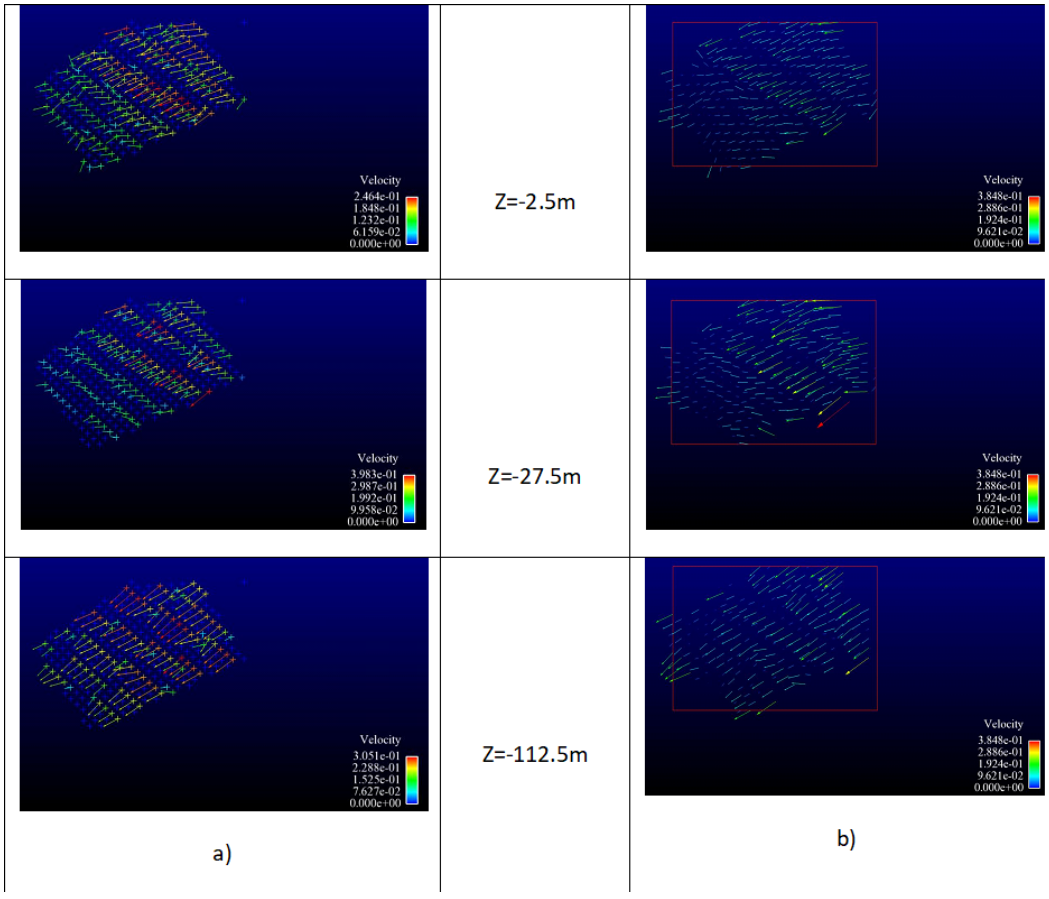

Figure 5. Tidal current at different coasts z at t = 17 hours: a) seeding points b) tetrahedral mesh.

5. Sedimentation rate model

For purposes of analysis of the dispersion of the OMA, the sedimentation velocity was superimposed field hydrodynamics. The magnitude of the sedimentation velocity is estimated

from the particle Reynolds number for a single particle (Bird et al., 2002). In this case, the particle Reynolds number is defined by:

$$Re_p = (\rho_l D_p v_s)/\mu_l \tag{3}$$

Where ρ_l and μ_l are respectively the density and viscosity of the liquid in this case the water in our case. Table 2 reproduces the values Reynolds number of particle that happen to be very small ($Re_p < 10^{-3}$)and indicate a sedimentation regime Stokes ($Re_p < 0.2$) In this case, the sedimentation rate is defined as:

$$v_s = \frac{(D_p^2 g)((\rho_s - \rho_l))}{18\mu_l} \tag{4}$$

Where ρ_s is the density of the particle and g the gravity ($g = 9.81 m/s^2$).

	Density of OMA ($d = 1.07$)			
$Dp(\mu m)$ ($\bar{D}_P = 200\mu m$)	1.01	1.05	1.10	1.15
50	$7.01\,10^{-8}$	$3.65\,10^{-7}$	$7.64\,10^{-7}$	1.2010^{-6}
125	$1.10\,10^{-6}$	$5.70\,10^{-6}$	$1.19\,10^{-5}$	$1.87\,10^{-6}$
250	$8.77\,10^{-6}$	$4.56\,10^{-5}$	$9.55\,10^{-5}$	$1.50\,10^{-4}$

Table 2. Values of Reynolds number for particle classes selected OMA

Table 3 presents the values of sedimentation rate for classes of OMA deductions obtained by directly applying equation (4). The amplitude varies between $1.39\,10^{-6} m/s$ and $5.21\,10^{-4} m/s$. In general, the higher the density increases, the sedimentation rate increases. Similarly, the larger the diameter increases, the sedimentation rate increases.

	Density of OMA ($d = 1.07$)			
$Dp(\mu m)$ ($\bar{D}_P = 200\mu m$)	1.01	1.05	1.10	1.15
50	$1.39\,10^{-6}$	$6.94\,10^{-6}$	$1.39\,10^{-5}$	2.0810^{-5}
125	$8.68\,10^{-6}$	$4.34\,10^{-5}$	$8.68\,10^{-5}$	$1.30\,10^{-4}$
250	$3.47\,10^{-5}$	$1.74\,10^{-4}$	$3.47\,10^{-4}$	$5.21\,10^{-4}$

Table 3. Values of the sedimentation velocity (m/s) for selected classes of OMA.

6. RESULTS

6.1. Injection conditions

Given the extent of the area and variability of field and hydrodynamic evaluation of the potential we have chosen several injection points. Figure 6 shows the position of the 6 injection points retained is designated by P1, P2 to P6. The points P1 and P4 are close to Matane. The point P2 is at the center of the river in the upstream part. The point P3 is Prees Mont-Joli. Points P5 and P6 are located near the north shore near the localities respectively Pointe-des-Monts Pointe-aux-Bustards. Cartesian coordinates and geographical points of injection are presented in Table 4.

points d'injection	X	Y	Z	*longitude*	*laltitude*
$P1$	298293.061608463	5426228.12238671	-12.875	$-67,58889$	$48,974277$
$P2$	233889.155792414	5397783.50334515	-17.875	$-68,463707$	$48,714474$
$P3$	241666.128377314	5384248.98750464	-21.875	$-68,355965$	$48,593601$
$P4$	278884.094407558	5404030.60395492	-36.875	$-67,852623$	$48,774147$
$P5$	316554.349939784	5462168.3409067	-3.875	-67.338379	49.297398
$P6$	245746.017524661	5433284.61726884	-105.875	$-68,307709$	$49,034943$

Table 4. Cartesian coordinates and geographical points of injection.

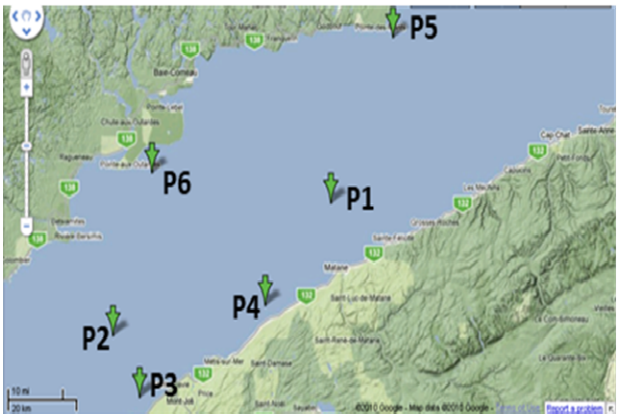

Figure 6. Geographical location of injection points for OMA in the study area (source Google Map).

The injection point type is represented by a hollow sphere of radius 1.0 m covered by a set of particles. The center of gravity of the sphere is immersed to about 2.0m below the free surface. Each class is represented by OMA population of 121 particles. In addition, each injection scenario is represented by the number of classes of OMA, 12, multiplied by the number of particles per class, OMA 121, which corresponds to a total population of 1452 particles for each scenario injection.

6.2. Duration of the dispersion-time calculation

For each class of OMA, the dispersion calculations were performed to predict the state dispersion for each day over a total period of 10 days. For the entire dispersion modeling program of OMA, 72 simulations per day dispersion (simulations are 720 in total for 10 days of follow-up) were launched on the Super computer SGI XE320 Network Quebecers High Performance Computing (RQCHP). To each simulation, the average running time is 13 to 16 CPU hours.

6.3. Trajectory of a particle

Preliminary tests have necessitated the search for numerical parameters in particular the number of shots per element that we finally set at 8000. We found that this value can predict the trajectory with good accuracy. In other words, a path OMA is calculated on the basis of 8000 points per finite element visited. Figure 7 shows the trajectory of a single particle.

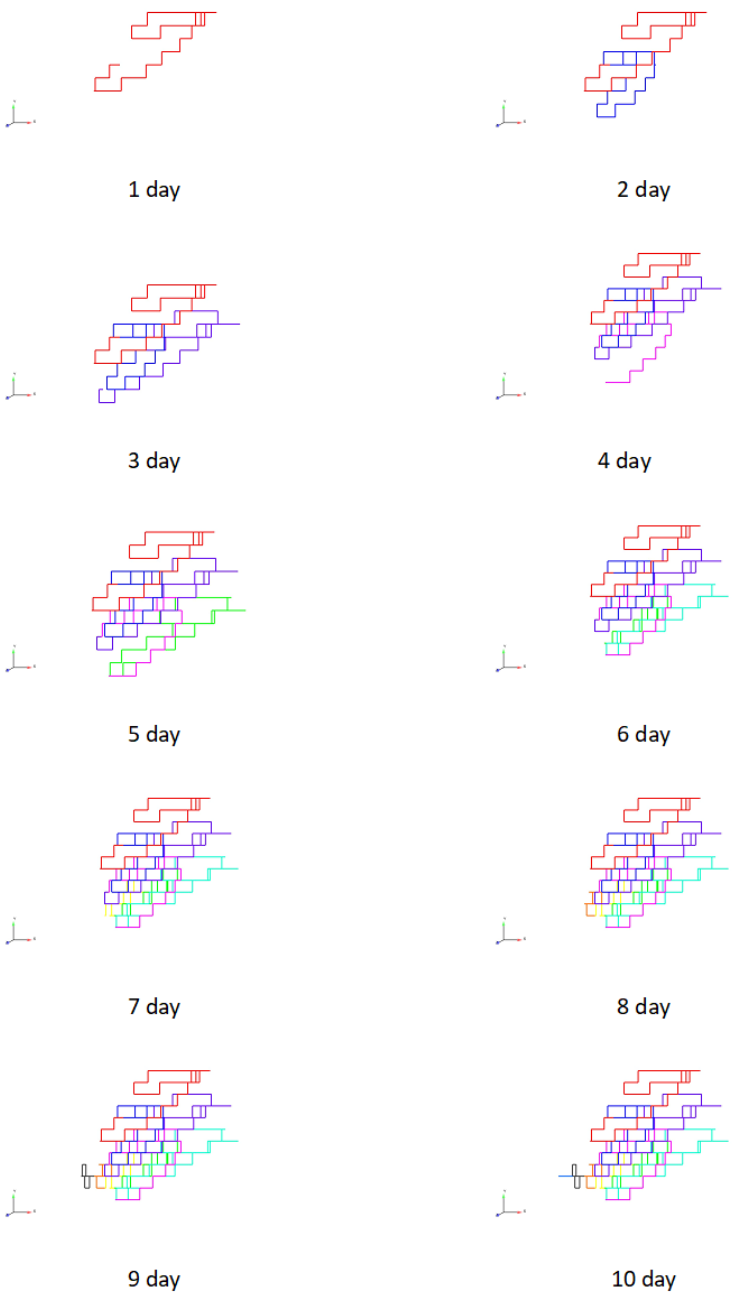

Figure 7. Trajectory of a particle for a period ranging from 10 days.

Under the effect of the tide, the course looks set to move back and forth, an expected result, with a tendency to drift toward the southwest. The shape of the jerky trajectory is probably due to the precision of the hydrodynamic time step of the order of the day, a smaller time step would probably have to have a smoother shape.Note that we get the same trajectory for values

of the number of shots over 8000.

The migration of OMA $P6$ is very different compared to other injection points. A justification for this difference is the greater variability of the current as shown in Figure 15a-b which shows the current in the vicinity of $P2$ and ditto for Figure 15c-d near the point $P6$ at $t = 1\,hour$ and $t = 3\,hours$ respectively. There is a drastic change in the current direction in which the $P6$ OMA migrate in both directions for Southwest OMA light and Northwest intermediaries while the heavier sediment.

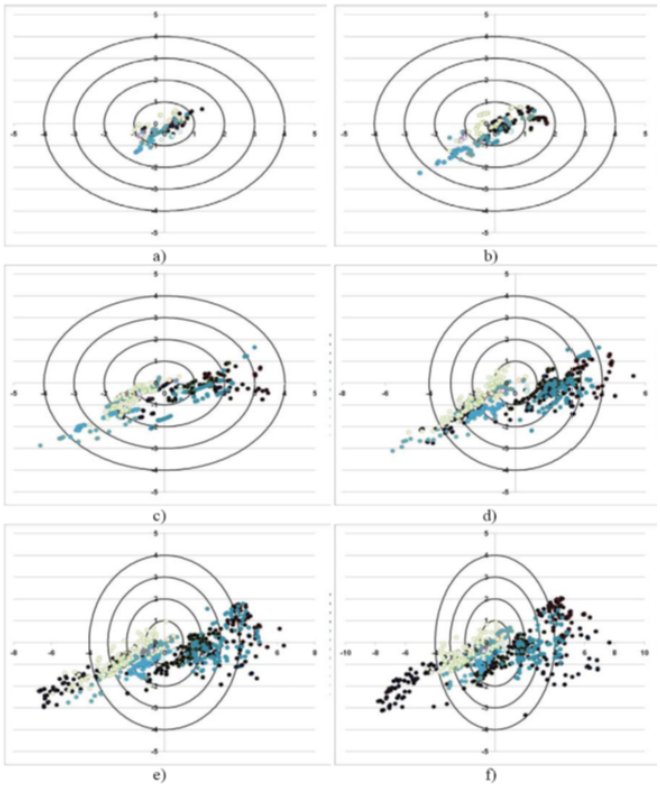

Figure 8. Dispersion of OMA from the point P1 on day: 1 (a), 2 (b), 4 (c), 6 (d), 8 (e) and 10 (f).

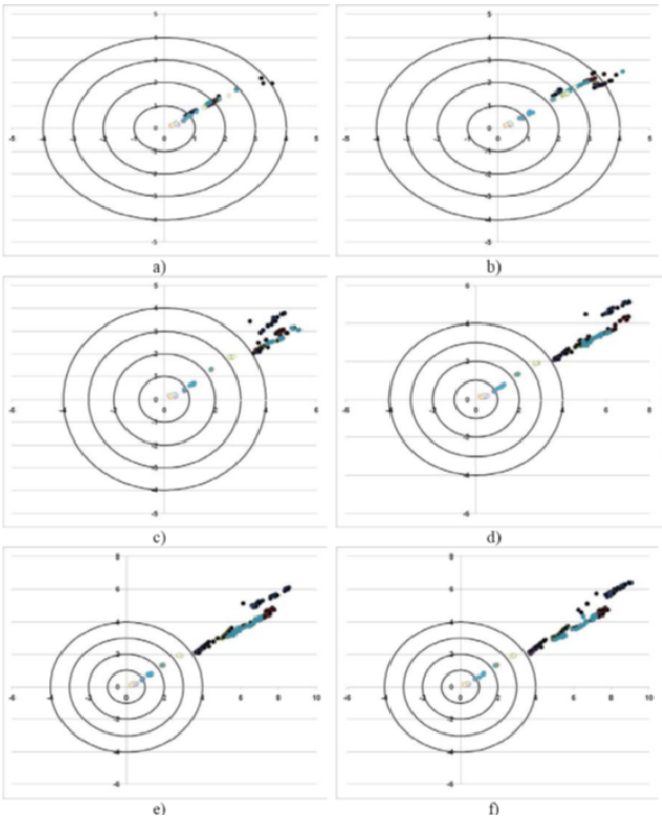

Figure 9. Dispersion of OMA from the point P2 on day: 1 (a), 2 (b), 4 (c), 6 (d), 8 (e) and 10 (f).

Although in Figure 8 to Figure 13, the particles move within a radius of about $5-6$ km, it is worth noting that like the Figure 7 the OMA cover a much greater distance, as confirmed Table 5 brings together all classes of OMA combined values of minimum and maximum distance recorded after 10 days of migration. Curiously, the point $P2$, which however is in the middle of the fairway, not the one who creates the longest course in OMA. Indeed, Figure 15 shows the weighted average distance traveled by the OMA from different sites.It is a journey of about 5 km after 10 days from the points $P2$, $P3$ and $P4$. As for the points P6, P1 and P5 are respectively 11, 19 and 22 km.

	Distance(km)	
location	min	max
$P1$	2.1	39.5
$P2$	0.9	18.3
$P3$	0.4	24.9
$P4$	1.9	10.1
$P5$	4.2	39.0
$P6$	2.2	26.8

Table 5. Minimum and maximum distance traveled by the OMA after 10 days.

Now we propose to measure the extent of migration that we express as an effective area

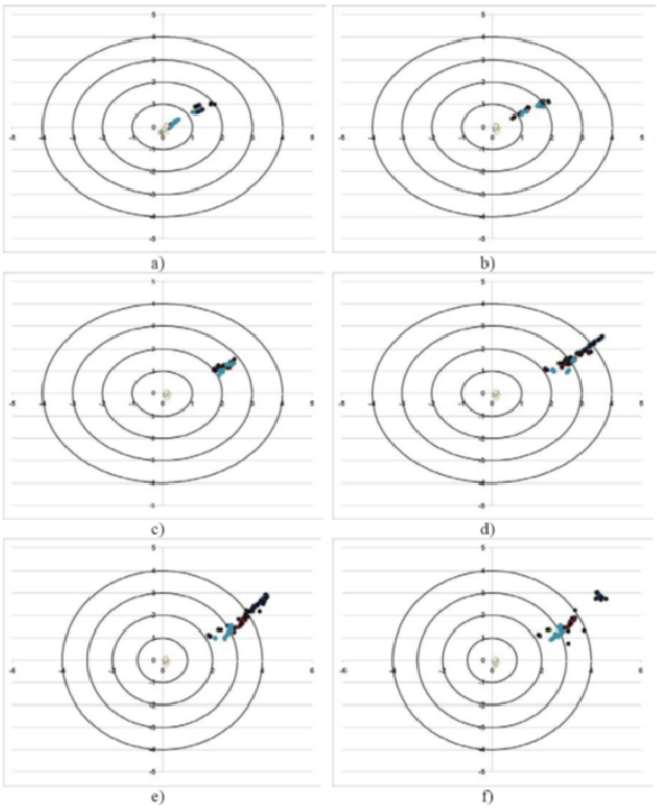

Figure 10. Dispersion of OMA from the point P3 on day: 1 (a), 2 (b), 4 (c), 6 (d), 8 (e) and 10 (f).

function of time and we denote by $S_{eff}(t)$ which is determined as follows:

$$S_{eff}(t) = |\max x(t) - \min x(t)||\max y(t) - \min y(t)| \tag{5}$$

Where $x(t)$ and $y(t)$ are vectors of coordinates in time of all classes of OMA.

The results of the spreading of the sheet of OMA are shown in Figure 16 with time as abscissa and the surface $S_{eff}(t)$ ordinate, it is interesting to note that the effective area increases monotonically with the exception of P2 increase is accompanied by an oscillation likely due to the tide which ebbs and flows in periodically tends to slow its expansion. Initially, the area covered by the sheet is less 1m2. We see that from the points P3 and P4 it reaches up to 10 km2, this double value from the point P6. It was from the injection points P1, P2 and P5 it is the largest, reaching from point P5 to 60 km^2.

6.4. Homogeneity of the dispersion

Examination of Figure 8 to Figure 13 shows a segregation of OMA that we propose to quantify. For this, we define the notion of area ratio denoted r(t), called the coefficient of homogeneity thereafter, and defined as follows:

$$r(t) = \frac{S(t)}{S_{eff}(t)} \tag{6}$$

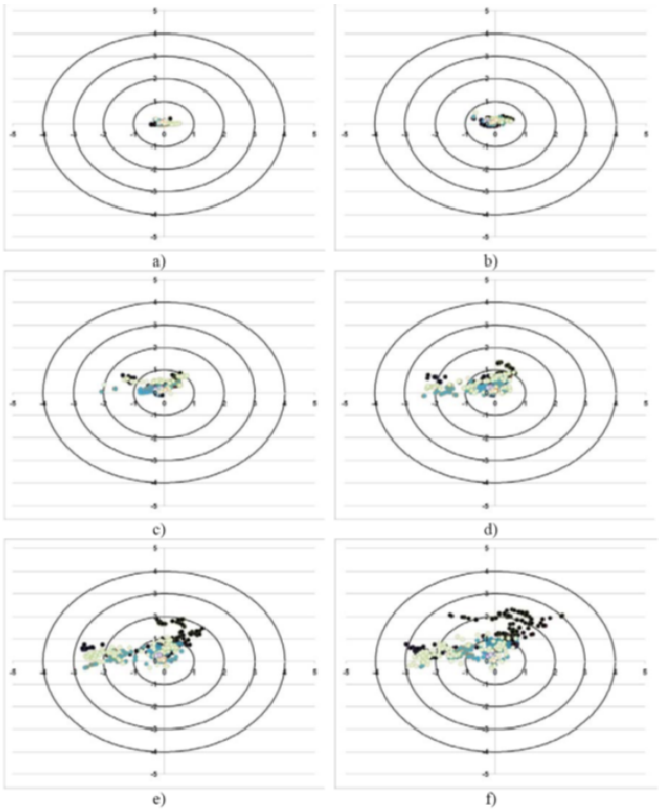

Figure 11. Dispersion of OMA from the point P4 on day: 1 (a), 2 (b), 4 (c), 6 (d), 8 (e) and 10 (f).

Where $S(t)$ is the surface of the OMA is given by the following equation:

$$S(t) = \sum_{i=1}^{12} p_i S_i(t) \tag{7}$$

Where the weights p_i, presented to the panel, follow the normal distribution and are associated with each class of each OMA which occupies an area $S_i(t)$ corresponding. The determination of $S_i(t)$ is obtained by:

$$S_i(t) = |\max x_i(t) - \min x_i(t)||\max y_i(t) - \min y_i(t)| \tag{8}$$

Exploit the values of $S(t)$ presented above to calculate the homogeneity coefficient $r(t)$. Emphasize, however, that when $r(t)$ tends to 1 the homogeneity of the OMA is an ideal distribution (Danckwerts, 1952). Otherwise, ie when $r(t)$ tends to 0, the distribution of OMA is completely segregated.Figure 17 shows a semi-log scale the evolution of the coefficient of homogeneity of the water injection point for each test. The homogeneity of the water deteriorates, considering that initially it is perfectly homogeneous ($r(t) = 1$) and stabilizes from the 2nd day. We note that for the injection points $P5$, $P1$, $P6$ and $P4$ (listed in descending order of consistency) the level of homogeneity is substantially the same. The web reached the level of homogeneity worst from the points $P2$ and $P3$. Figure 17.

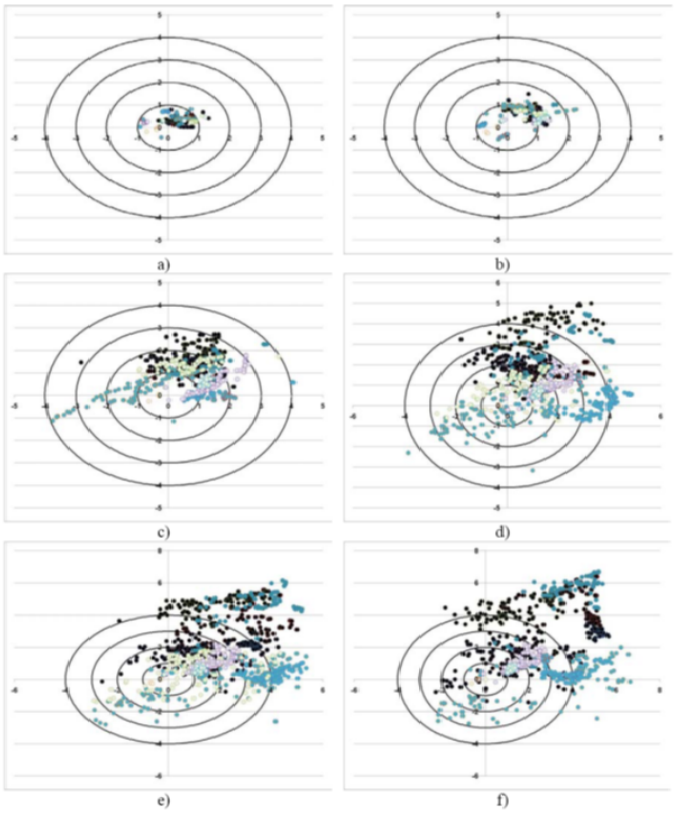

Figure 12. Dispersion of OMA from the point P5 on day: 1 (a), 2 (b), 4 (c), 6 (d), 8 (e) and 10 (f).

6.5. Occupation of the water column by the OMA

The evolution of the occupation of the water column by the OMA from the injection sites $P1$, $P2$, $P3$, $P4$, $P5$ and $P6$, respectively, is presented in Figure 18 to Figure 23. The Migration is presented as positions of particles on a plane (rz) admitting radial direction (from the injection site) on the abscissa and the vertical direction ordered. The unit of length is kilometer (km) along the radial direction and meter (m) in the vertical direction. The origin corresponds to the point of injection. The position of OMA is presented for days 1, 2, 4, 6, 8 and 10. Sediment plumes are different from one injection to another. Except point P2 (channel), there is a distinct phenomenon of sedimentation for all points injection. Point P3 is the injection point from which there is a plume dispersion most segregated. The denser particles settle at the end of day 1 and found at a depth of 300m. From the results of the spreading surface and depth we OMA able to determine changes in concentration of OMA that we study in next section, remember that concentration is an important indicator of quality water. The higher the concentration of OMA is the better the low dispersion. In this case the middle is able to assimilate the OMA with micro-organisms. Evolution of the concentration of OMA over 8000.

The migration of OMA $P6$ is very different compared to other injection points. A justification for this difference is the greater variability of the current as shown in Figure 15a-b which shows the current in the vicinity of $P2$ and ditto for Figure 15c-d near the point $P6$ at $t = 1\,hour$ and $t = 3\,hours$ respectively. There is a drastic change in the current direction in which the $P6$ OMA migrate in both directions for Southwest OMA light and Northwest intermediaries while the heavier sediment.

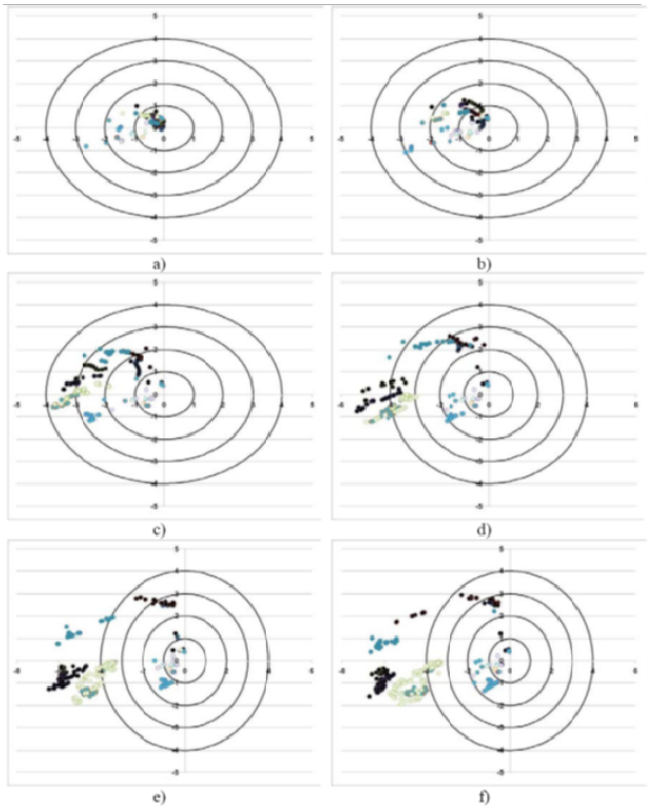

Figure 13. Dispersion of OMA from the point P6 on day: 1 (a), 2 (b), 4 (c), 6 (d), 8 (e) and 10 (f).

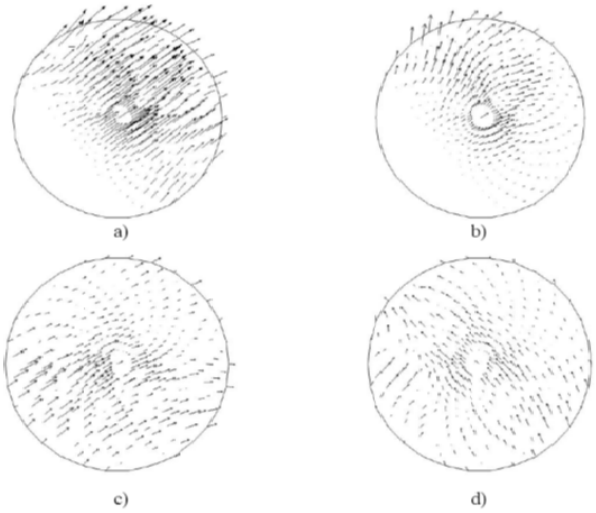

Figure 14. Running to the side of the injection point (z =- 3.875m) in a 5 km radius around the point P2 at t = 1.00 hour (a) and t = 3.00 hour (b) and around the point P6 at t = 1.00 hour (c) and t = 3.00 hour (d).

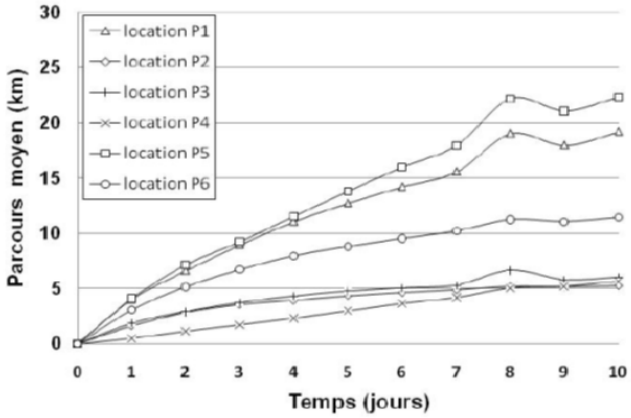

Figure 15. Average length of OMA from different sites.

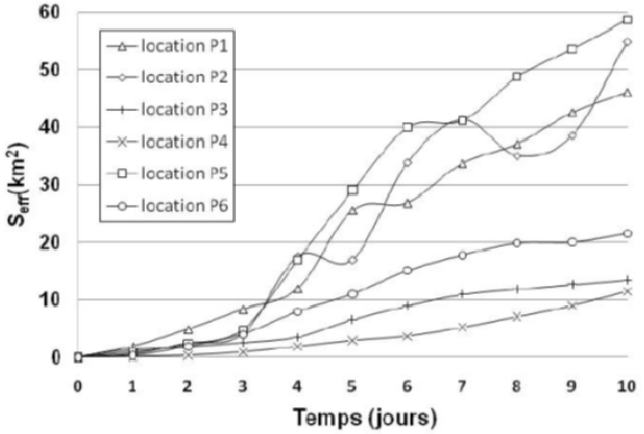

Figure 16. Surface area of OMA.

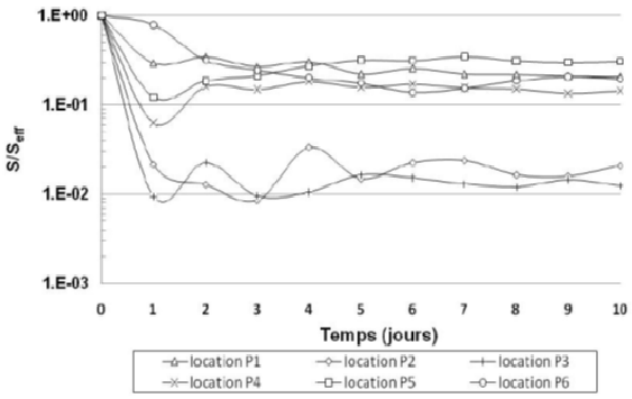

Figure 17. .

Figure 18. Evolution of the sedimentation of OMA from the point P1 on day: 1 (a), 2 (b), 4 (c), 6 (d), 8 (e), 10 (f).

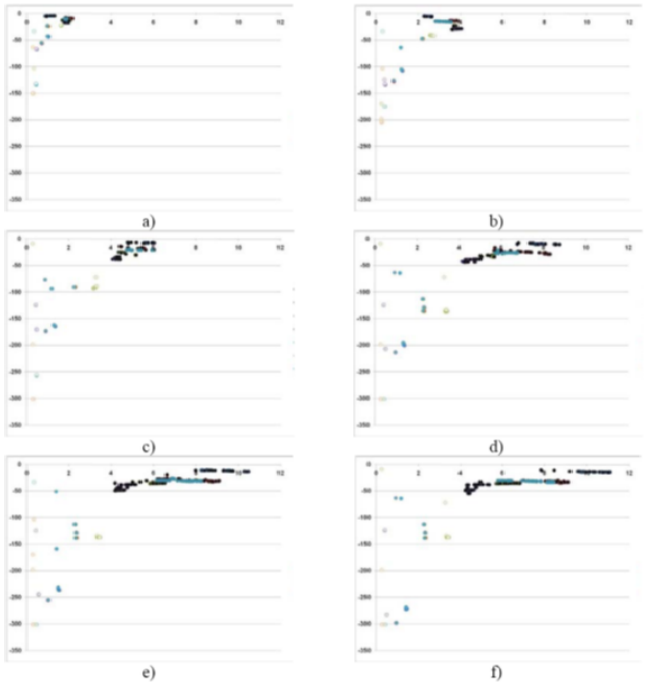

Figure 19. Evolution of the sedimentation of OMA from the point P2 on day: 1 (a), 2 (b), 4 (c), 6 (d), 8 (e), 10 (f).

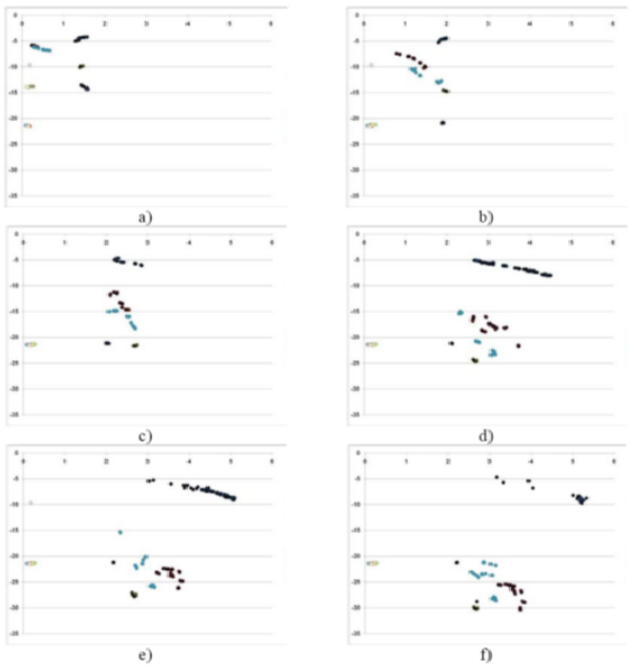

Figure 20. Evolution of the sedimentation of OMA from the point P3 on day: 1 (a), 2 (b), 4 (c), 6 (d), 8 (e), 10 (f).

Figure 21. Evolution of the sedimentation of OMA from the point P4 on day: 1 (a), 2 (b), 4 (c), 6 (d), 8 (e), 10 (f).

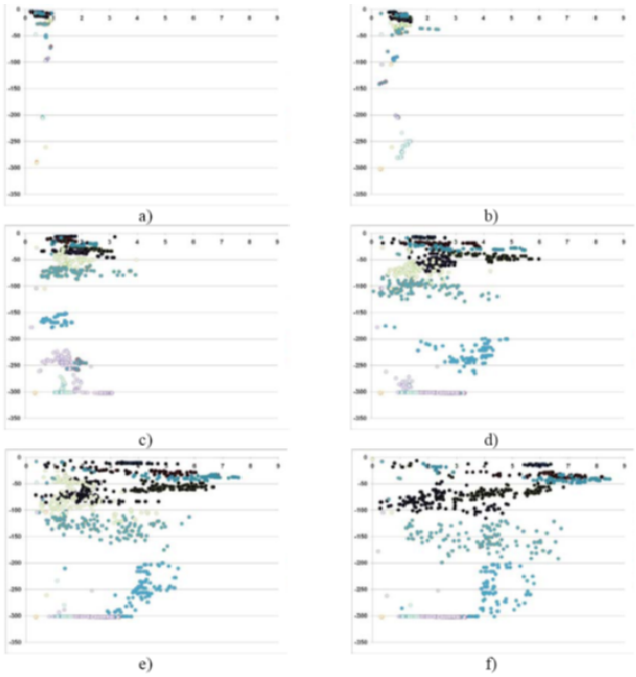

Figure 22. Evolution of the sedimentation of OMA from the point P5 on day: 1 (a), 2 (b), 4 (c), 6 (d), 8 (e), 10 (f).

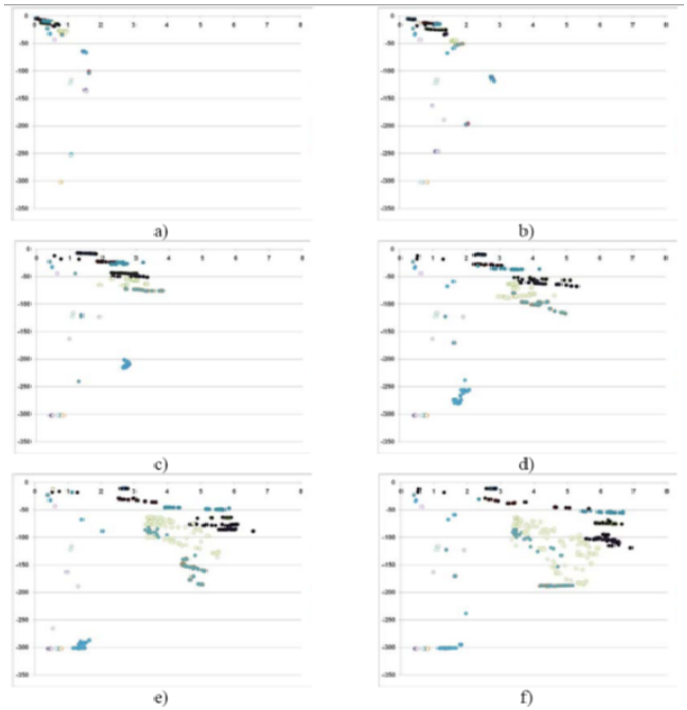

Figure 23. Evolution of the sedimentation of OMA from the point P5 on day: 1 (a), 2 (b), 4 (c), 6 (d), 8 (e), 10 (f).

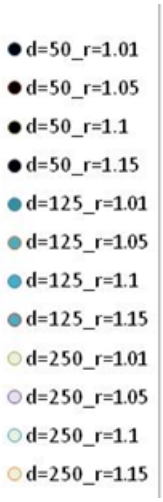

Figure 24. OMA class legend.

In addition to sprawl, it is interesting to know the evolution of the concentration $C(t)$ OMA starting from the initial concentration $C(0)$ which is a priori unknown. By cons, we can measure the concentration ratio:

$$\frac{C(t)}{C(0)} = \frac{M}{V(t)}\frac{V(0)}{M} = \frac{V(0)}{V(t)} \tag{9}$$

The initial volume of OMA $V(0)$ is known as imposed. The volume at time t is obtained by simulation and is determined, like dispersion, by:

$$V(t) = \sum_{i=1}^{12} p_i V_i(t) \tag{10}$$

where $V_i(t)$ are the volumes associated with each class of OMA.

$$V_i(t) = S_i(t)|\max z_i(t) - \min z_i(t)| \tag{11}$$

Note here that M is the mass of OMA, which is assumed constant (conservative contaminant). If there is degradation, the mass OMA decreases over time. Keeping M constant corresponds to a less optimistic scenario.

Figure 24 shows a semi-log scale the evolution of the concentration ratio $C(t)/C(0)$ from the points of injections for 10 days of simulation. It is interesting and reassuring an environmental point of view, to note that from all points of injection, the concentration ratio decreases exponentially indicating a dilution of the burden of ABS. The decrease was significant in the first days and slows beyond. For example, the first day the value of $C(t)/C(0)$ goes from 1 to 10^{-6}.Dispersion coefficients From the injection sites selected under this study, we were interested in quantifying the dispersion coefficients of horizontal and vertical OMA. In practice, the coefficient of horizontal dispersion can easily predict the evolution in terms of the spread sheet

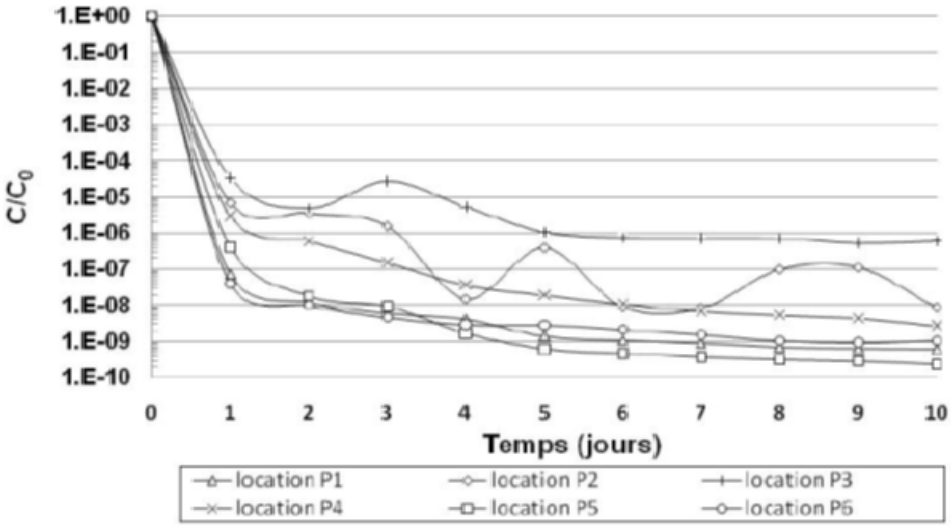

Figure 25. Evolution of the sedimentation of OMA from the point P6 on day: 1 (a), 2 (b), 4 (c), 6 (d), 8 (e), 10 (f).

of OMA. Similarly, the vertical dispersion coefficient allows for him to predict the progression of sedimentation. However, their determination by the approach proposed by Fisher et al. (1979) is demanding in data processing. To circumvent this difficulty, we propose to address the issue by a simplified approach that we outline below. The dispersion process as determined by equation (1) is of convective nature. It can be approached by a diffusion phenomenon, which admits a one-dimensional analytical solution. Indeed, consider a scalar U governed by partial differential equation follows:

$$\frac{\partial u}{\partial t} - k\frac{\partial^2 U}{\partial \zeta^2} = 0 \tag{12}$$

where k is the coefficient of dispersion and ζ coordinate the dispersion axis we define as follows:

- Horizontal dispersion: $\zeta = \sqrt{((x-x_p)^2 + (y-y_p)^2)}$ with (x_p, y_p)-coordinate of the point injection.
- vertical dispersion $\zeta = z$ and $\zeta = z - z_p$ with z_p the coast of the point injection.

The analytical solution of (8) has the form:

$$U(\zeta, t) = \frac{U(0)}{2\sqrt{nkt}} e^{\frac{-\zeta^2}{4kt}} \tag{13}$$

The values of dispersion coefficients were determined from a regression on Simulation results of S and C are presented in Table 6. An examination of values Table 6 shows that the vertical dispersion coefficient is more regular and important than horizontal dispersion. This seems a consistent result in that hydrodynamics is almost horizontal, while vertical flow is secondary. They are between 1.18310^{-4} and $210.5m^2/s$ for the horizontal dispersion and between 118.0 and $296.3m^2/s$ for vertical dispersion. It is worth noting that these values are in the same vein as those established by Ahsen (2008). It should be noted that the sensitivity of the determination coefficients dispersal in natural environment is important and it is not excluded that the error is of the order of ± 100

	Coefficients de dispersion (m^2/s)	
location	*Horizontal*	*vertical*
$P1$	1.58110^2	1.18010^2
$P2$	2.10510^2	1.34210^2
$P3$	1.18310^{-4}	2.96310^2
$P4$	1.02610^1	1.96110^2
$P5$	5.341	2.22210^2
$P6$	3.33310^1	1.66710^2

Table 6. Minimum and maximum distance traveled by the OMA after 10 days.

7. Conclusion

This study has highlighted the potential for dispersal of OMA on the St. Lawrence River in the region of Matane. Different criteria were used to analyze the dispersion of OMA with the weighted area of contamination, the effective area of contamination, the coefficient homogeneity, the occupation of the water column and the concentration of contaminant conservative. Also, a simplified method based on horizontal and vertical dispersion to easily quantify the evolution of the dispersion is proposed. The dispersion analysis was performed using 6-point injection. The results showed a great diversity of facies dispersion. It seems obvious that analysis of dispersion should be on a case by case basis. However, the majority of injection sites tested showed that the contamination is diluted significantly over a period of 10 days. The maximality criterion for determining the dispersion is, in our humble opinion, based on intervention on the ground

8. ACKNOWLEDGEMENTS

The authors wish to express their sincere thanks to the Quebec Network Computing High Performance (RQCHP) and Compute Canada for access to super computers for completion of this work.

[1] Ahsen, N. (2008). Estimating the coefficient of dispersion for a natural stream. World Academy of Science, Engineering and Technology, 44:131-135.

[2] Bird .R.B, Stewart .W .E, Lightfoot E. N.(2002). Transport phenomena, Second Edition,John Wiley and Sons, Inc.

[3] Bragg, J.R. and Yang, S.H. (1995) Clay-oil flocculation and its role in natural cleaning in Prince William Sound following the Exxon Valdez oil spill. In Exxon Valdez Oil Spill: Fate and Effects in Alaskan Waters, P.G. Wells, J.N. Butler and Hughes, J. S. Eds.), American Society for Testing and Materials, Philadelphia, Pennsylvania, 178-214.

[4] Cheng, H.-P., Cheng, J.R., Yeh, G.T. (1996). A particle tracking technique for the Lagrangian-Eulerian finite element method in multi-dimensions. International Journal for Numerical Methods in Engineering, 39(7): 1115-1136.

[5] Cloutier, D., Doyon, B. (2008) OMA formation in ice-covered brackish waters: Large-scale experiments, NATO Science for Peace and Security, Series C: Environmental Security, 71-88. Cooley, J.W., Tukey, J.W. (1965). An algorithm for the machine calculation of complex Fourier series. Mathematics of Computation, 19(90): 297-301.

[6] Devals, C., Doyon B., Heniche M. (2009). Modelling of the dispersion of oil-mineral aggregates in ice-infested waters. In the Proceeding of the 8th World Congress of Chemical Engineering, Montréal QC Canada.

[7] Fisher, H. B., List, E.J., Koch, R.C.Y., Imberger, J., Brooks, N.H. (1979). Mixing in inland and coastal waters, Academic Press Inc.

[8] Heniche, M., Tanguy, P.A. (2006). A new element-by-element method for trajectory calculations with tetrahedral finite element meshes. International Journal for Numerical Methods in Engineering, 67:1290-1317.

[9] Hill, P.S., Khelifa, A., Lee, K. (2002) Time scale for oil droplet stabilization by mineral particles in turbulent suspensions. Spill Science and Technology Bulletin; 8(1):73–81.

[10] Khelifa, A., Stoffyn-Egli P., Hill P.S., Lee, K. (2002) Characteristics of oil droplets stabilized by mineral particles: effects of oil type and temperature. Spill Science and Technology Bulletin; 8(1):19–30.

[11] Leclerc, M., Boudreau, P. (1993) Lagrangian modeling of water quality and contamination analysis of a St. Lawrence River reach: Lake St. Pierre (Canada). Revue des Sciences de l'Eau; 6:427-452.
[12] Niu, H., Li, Z., Lee, K.,Kepkay, P., Mullin, J.V. (2011) Modelling the transport of oil–mineral-aggregates (OMAs) in the marine environment and assessment of their potential risks. Environ Model Assess, 16:61–75.
[13] Sayed, M., Serrer, M., Mansard, E. (2008) Oil spill drift and fate model. Book chapter in W. F. Davidson, K. Lee and A. Cogswell (eds.), Oil Spill Response: A Global Perspective, Springer Netherlands, 205-220.
[14] Wilcox, D.C. (2004) Turbulence Modeling for CFD. La Cañada: DCW Industries.